

High-Speed Charge-to-Time Converter ASIC for the Super-Kamiokande Detector

H. Nishino^{a,*}, K. Awai^a, Y. Hayato^a, S. Nakayama^a, K. Okumura^a,
M. Shiozawa^a, A. Takeda^a, K. Ishikawa^b, A. Minegishi^b, Y. Arai^c

^a*Institute for Cosmic Ray Research, University of Tokyo, Chiba 277-8582, Japan*

^b*Iwatsu Test Instruments Corporation, Tokyo 168-8511, Japan*

^c*The Institute of Particle and Nuclear Studies, KEK, Ibaraki 305-0801, Japan*

Abstract

A new application-specific integrated circuit (ASIC), the high-speed charge-to-time converter (QTC) IWATSU CLC101, provides three channels, each consisting of preamplifier, discriminator, low-pass filter, and charge integration circuitry, optimized for the waveform of a photomultiplier tube (PMT). This ASIC detects PMT signals using individual built-in discriminators and drives output timing signals whose width represents the integrated charge of the PMT signal. Combined with external input circuits composed of passive elements, the QTC provides full analog signal processing for the detector's PMTs, ready for further processing by time-to-digital converters (TDCs). High-rate (>1 MHz) signal processing is achieved by short-charge-conversion-time and baseline-restoration circuits. Wide-range charge measurements are enabled by offering three gain ranges while maintaining a short cycle time. QTC chip test results show good analog performance, with efficient detection for a single photoelectron signal, 4 orders of magnitude dynamic range (0.3 mV \sim 3 V; 0.2 \sim 2500 pC), 1% charge linearity, 0.2 pC charge resolution, and 0.1 ns timing resolution. Test results on ambient temperature dependence, channel isolation, and rate dependence also meet specifications.

Key words: Super-Kamiokande, photomultiplier tube readout, charge-to-time converter, self-trigger, high-speed, low-noise

*Corresponding author. Tel.: +81 471 36 3130; fax: +81 471 36 3126.

Email addresses: nishino@post.kek.jp (H. Nishino)

¹Present address: The Institute of Particle and Nuclear Studies, KEK, Ibaraki 305-0801, Japan

1. Introduction

Super-Kamiokande (SK) is the world's largest ring-imaging water Cherenkov detector for astroparticle and elementary particle physics. In operation since 1996, it has achieved several important scientific results, notably discovery of neutrino flavor mixings and their masses [1, 2]. The detector will stay in operation to further explore atmospheric and solar neutrinos, artificial neutrinos in an accelerator-based long baseline neutrino experiment [3], cosmic neutrinos from supernova explosions [4], baryon-number-violated proton decay signals [5], and more.

The 50 kt cylindrical water tank shown in Fig. 1, 39 m in diameter and 42 m in height, houses an inward-facing array of 50-cm photomultiplier tubes (PMTs) and outward-facing array of 20-cm anticounter PMTs. The former array consists of 11,129 HAMAMATSU R3600 hemispherical PMTs; the latter array consists of 611 R1408 and 1274 R5912 PMTs. Details of the detector and its data acquisition electronics are reported elsewhere [6, 7]. The SK collaboration decided to replace detector's front-end electronics with new ones, which motivated the development of a new device as described herein.

It is required that front-end electronics for the detector record the integrated charge of the PMT signals and their timing, corresponding to the amount of detected Cherenkov light and its time of arrival on the PMT surface, respectively. Each channel self-triggers—that is, starts charge integration by itself using its own discriminator—because an external start timing signal is not available for natural neutrino and proton decay observations. The electronics also match the characteristics of the PMTs; the R3600 PMTs operate with a gain of 10^7 and their signals are transported to the electronics via 70-m RG58 coaxial cables. The charge dynamic range of the PMT is ~ 1000 photoelectron (p.e.; plural p.e.s).

Figure 2 shows the waveform of a single p.e. signal from an R3600 PMT. Charge and timing resolution of the PMT at the single p.e. level ($\simeq 2$ pC) are about 100% and 2 – 3 ns, respectively [8], and the single p.e. signal should be detected with high efficiency at a discriminator threshold of $\sim 1/4$ p.e.s. A short ($< 1 \mu\text{sec}$) cycle time is required to record, with high efficiency, two successive events in which Michel electron events follow muon events with a mean interval of the muon's lifetime, $2 \mu\text{sec}$.

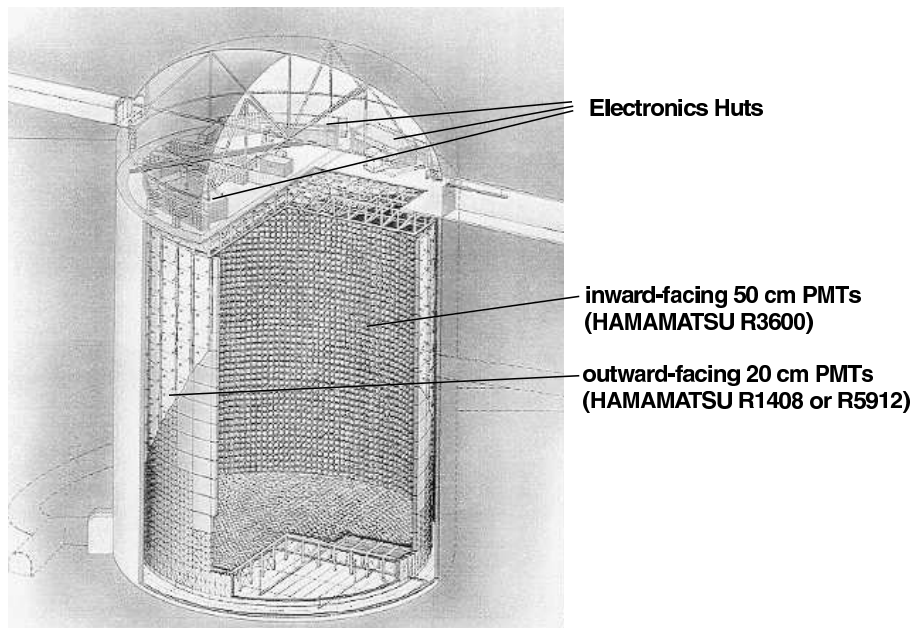


Figure 1: Sketch of the Super-Kamiokande detector.

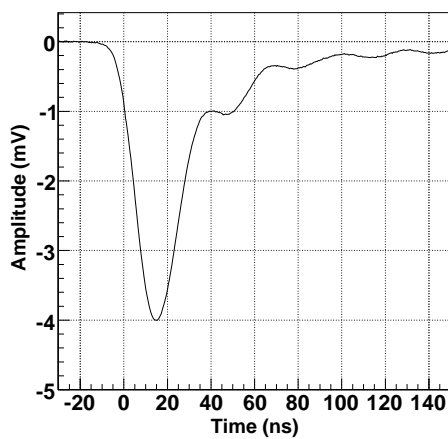


Figure 2: Waveform of single photoelectron signals of the R3600 PMT recorded at the end of a 70-m RG58 coaxial cable.

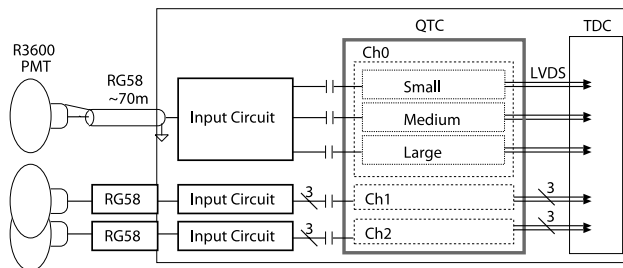


Figure 3: Block diagram of the QTC and its surroundings. PMT signals, transmitted through coaxial cables, are divided among three QTC gain ranges. Combined with the input circuits, the QTC provides full analog signal processing for the PMT signals. Output signals are generated by LVDS drivers and read by TDCs.

For long-term operation of the SK detector, an integrated 3-channel device for PMT signal readout has been developed. This application-specific integrated circuit (ASIC), called the high-speed charge-to-time converter (QTC) IWATSU CLC101, was designed in CMOS $0.35\ \mu\text{m}$ technology. It has built-in discriminators to trigger its integration circuits by itself, and encodes the amount of input charge to the timing signal, where leading edge and width represent timing and integrated charge of the input signal, respectively. Necessary preamplifier and analog delay circuits also reside in the ASIC to enable high-density application.

The new ASIC offers three charge dynamic ranges, each with a short cycle time ($< 1\ \mu\text{sec}$). In real application, the output signal from each range would be digitized by modern time-to-digital converters (TDCs), e.g. the ATLAS Muon TDC ASIC [9] whose least significant bit (LSB) resolution is $0.52\ \text{ns}$. A field-programmable gate array (FPGA) would then choose which range is most appropriate and send only that one to be read by data acquisition computers.

In this article, section 2 describes the design of the new QTC ASIC. Section 3 describes the performance of the ASIC on the final fabricated chip. Section 4 presents our conclusions.

2. Design of the QTC ASIC

2.1. Overview of the design

Figure 3 shows a diagram of the QTC and its surroundings, and Table 1 summarizes its specifications. The QTC has three input channels per chip.

Each channel has three gain ranges: Small, Medium, and Large. The gain of each range can be adjusted by external resistor networks. The overall charge dynamic range of the QTC is 0.2 – 2500 pC if the gain ratio of three ranges is set to $1 : \frac{1}{7} : \frac{1}{49}$. Gains and ratios can be optimized to cover a wide dynamic range with reasonable resolution.

Figure 4 shows a block diagram of one QTC channel. Input signals from PMTs are amplified by a low-noise amplifier (LNA), delayed by a low-pass filter (LPF), processed by a voltage-to-current (V/I) converter, and integrated by a capacitor. The sum of the input-signal waveform to the capacitors can be monitored through an output signal designated PMTSUM.

The QTC is of the type of charge sensitive and a ramp or Wilkinson’s method is used for analog signal conversion. Charge integration starts when the amplified input signal crosses the discriminator threshold. The leading edge of the output signal represents this timing. Simultaneously, a trigger flag signal (HIT) is generated. After a charging period determined by the timer block, the integrated signal starts to be discharged by a constant current source. The discharging time is proportional to the integrated charge, which is known from the width of the output signal. Thus, the QTC output signal contains both timing and charge information.

Charge calibration is performed by the calibration signal path (CAL) and a forced trigger signal (PEDESTAL). Details of CAL are described in Section 2.2.2. The QTC output signal with null input signal can be measured by asserting the PEDESTAL signal.

The timer block contains three important timers: a charging timer, a discharging timer, and a VETO timer. These timers each generate timing gates by ramps with constant discharge current and comparators. The time length for these gates are controlled by digital-to-analog converters (DACs) for discharge current and for comparator threshold levels.

Figure 5 shows the timing chart for QTC operation. The charging timer, triggered by the discriminator output signal, operates for ~ 400 ns. Soon after the end of the charge gate, the discharging timer operates for ~ 350 ns. During the charge gate, the switch between the V/I converter and charging capacitor closes and input charge accumulates in the capacitor. During the discharge gate, the switch between the discharging current source and capacitor closes, and arriving input signals are ignored. The trailing edge of the QTC output signal represents the time when the integrated signal voltage decreases to the comparator threshold level; thus, the QTC output signal widens as the input signal gets larger. At the end of the discharge gate, reset

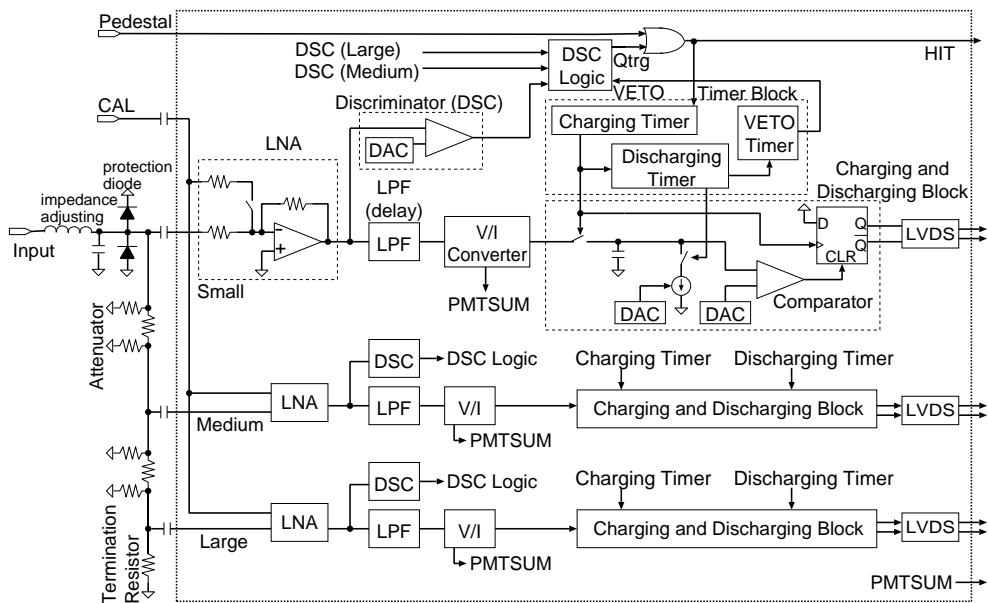


Figure 4: Block diagram of the one QTC channel. Each channel has 3 gain stages: Small, Medium and Large. Each stage is composed of several blocks: LNA, LPF, discriminator, V/I converter, and charging/discharging block. A single timer block serves all three ranges. PMTSUM is the analog sum of the output waveform of the V/I converter.

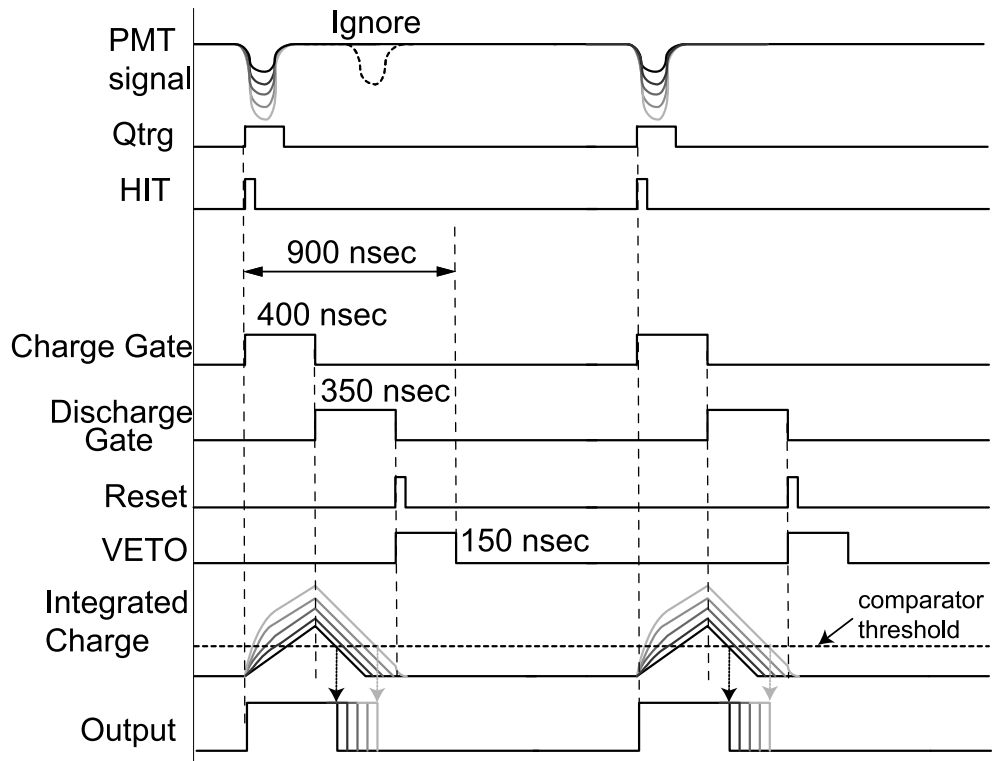


Figure 5: Timing chart for QTC operation. Gradation of the PMT signal corresponds to that of the integrated charge and the output. Widths of the charge and discharge gates are generated by ramps with constant discharge current and comparators, which can be controlled by register configurations. The total processing time for one hit is 900 nsec.

Table 1: Specification of the QTC

Type of trigger	self trigger by discriminator
Number of Input Channels	3
Processing Speed	~ 900 ns/cycle
Charge Integration Gate	400 ns
Number of Gains	3 (Ratio $1 : \frac{1}{7} : \frac{1}{49}$)
Discriminator Threshold	$-0.3 \sim -14$ mV (small range)
Charge Dynamic Range	$0.2 \sim 51$ pC (small) $1 \sim 357$ pC (medium) $5 \sim 2500$ pC (large)
Charge Resolution	~ 0.2 pC (small)
Integral (Non-)Linearity	$< \pm 1\%$
Timing Resolution	0.3 ns (2 pC, -3 mV) < 0.1 ns (> 100 pC)
Power Dissipation	< 100 mW/ch
Process	$0.35 \mu\text{m}$ CMOS
Package	100 pin CQFP

and VETO signals are issued. All QTC circuits except the VETO timer are reinitialized and the baseline of the LPF output is restored to avoid undesired effects for the next incoming signals. Input signals within ~ 150 ns after the discharge gate are ignored. In total, processing time for one input signal is ~ 900 ns.

Some QTC operations and gate lengths can be configured through register settings. The dynamic range of the gate length is $150 - 1000$ ns. The discriminator threshold is controlled by a DAC and by the gain of the discriminator's amplifier. The configurable discriminator threshold for the largest gain range (Small) is -0.3 to -14 mV. Which discriminator output among the three ranges is used to trigger charging is also determined by control registers. The discriminator threshold can be increased by using a lower gain range for the trigger. A channel can be disabled by disabling all three of its ranges. The charge dynamic range can be controlled by the gain of the V/I converter and the amount of constant discharge current; a larger discharge current produces less jitter and has a smaller charge dynamic range. Discharge current should be optimized to achieve the best resolution over the required dynamic range.

To minimize power consumption, the QTC is designed to operate with a

single +3.3 V power supply. The band gap reference of +1.2 V drives the internal bias circuit and built-in 6-bit/8-bit control DACs.

2.2. Design of the analog circuit

This subsection describes the analog circuits that are crucial to QTC performance, to handle accurate impedance matching at the input circuit block, wide-band signal amplification in the LNA, noise suppression by band limitation at the discriminator block, and signal delay by the LPF for precise charge integration.

2.2.1. External input circuit

As shown in Fig. 4, there is an external input circuit which contains a termination resistor, gain-adjusting attenuators, and DC blocking capacitors outside of the QTC. In order to satisfy the requirement for impedance matching at precision for $<0.1\%$ U-turned reflection signal, an external resistor network is used for the input signal termination while the QTC input impedance is 10 k Ω . This external resistor network is also used to determine the gains of the three QTC gain stages. In our application for the SK detector, input signals are divided by two 17 dB π attenuators into the three gain stages, for which the ratio of the divided signals is $1 : \frac{1}{7} : \frac{1}{49}$. Then the divided signals are fed into the QTC via the DC blocking capacitors to avoid direct current injection.

2.2.2. Low-noise amplifier

Figure 6 shows the LNA, which amplifies the input PMT signals. The LNA is a resistor feedback inverting amplifier with a cascode stage. Resistive rather than capacitive feedback is used to handle signals with wide bandwidth. The signal path CAL is devoted to charge calibration. A common calibration pulse can be supplied to all ranges of all channels. The path can be switched on and off by a MOSFET single-pole single-throw (SPST) switch controlled by register settings.

Figure 7 shows the simulated gain and equivalent input noise density of the LNA as a function of frequency. The low-frequency gain is 24 dB, and the 3-dB bandwidth is 60 MHz. In our simulation, PMT signals with a rise time of 10 ns are amplified without shape distortion when the quiescent bias current is as low as 2 mA, even with a high slew rate. The total equivalent input noise amplitude in a bandwidth from DC to 100 MHz is estimated to be 30 μ Vrms, equivalent to 1/100 p.e.s, sufficiently small for our applications.

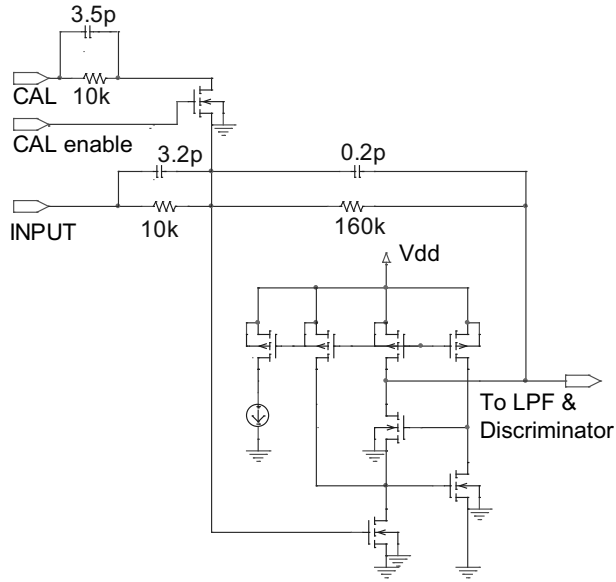


Figure 6: Simplified schematic of the LNA. The calibration signal path CAL can be switched on and off by the MOSFET switch. "CAL enable" is the control register signal for the switch.

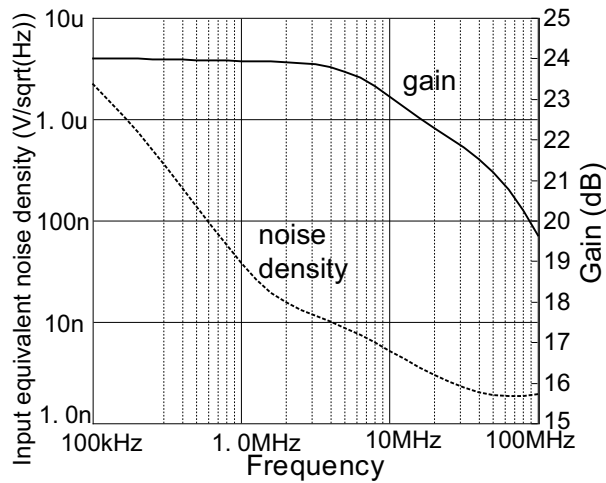


Figure 7: Simulated gain and equivalent input noise density of the LNA as a function of frequency.

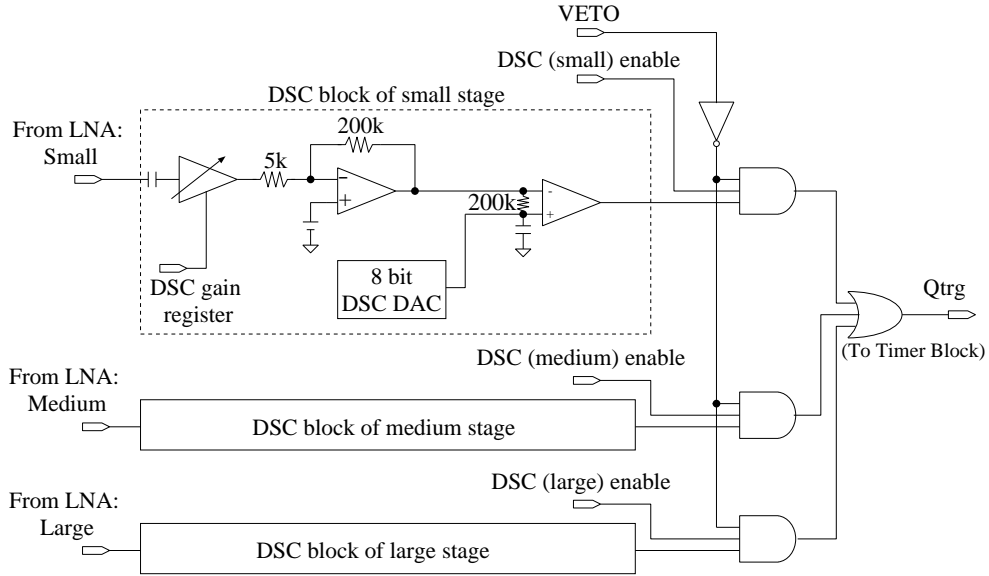


Figure 8: Schematic of the discriminator block. Each gain stage has an independent discriminator circuit. Which gain stage is used for the trigger source is determined by register settings.

2.2.3. Discriminator

Figure 8 shows that signals amplified at the LNA are fed into the discriminator block. At the first stage of the discriminator block, input signals are amplified again by a variable-gain amplifier and a fixed-gain amplifier.

Figure 9 shows the simulated results for gain and for equivalent input noise density for the amplifiers in the discriminator block. To suppress noise density in the lower-frequency region, the bandwidth of the amplifiers is optimized so that the lower and upper 3-dB cutoff frequencies are 5 and 30 MHz, respectively. The total equivalent input noise amplitude at the comparator is estimated to be $30 \mu\text{V}_{\text{rms}}$, equivalent to 1/100 p.e.s.

Timing jitter for the discriminator is determined by the noise voltage and the slew rate of the input signal. The equivalent input noise voltage of $30 \mu\text{V}_{\text{rms}}$ is amplified by 50 dB, resulting in an equivalent output noise voltage of 10 mV_{rms}. For a noise voltage of 10 mV and a maximum slew rate of 0.1 V/ns, we estimate the timing jitter to be 0.1 ns.

The discriminator threshold can be set by an 8-bit DAC with a step of $10 \mu\text{V}/\text{LSB}$. The dynamic range of the threshold can be enlarged to a

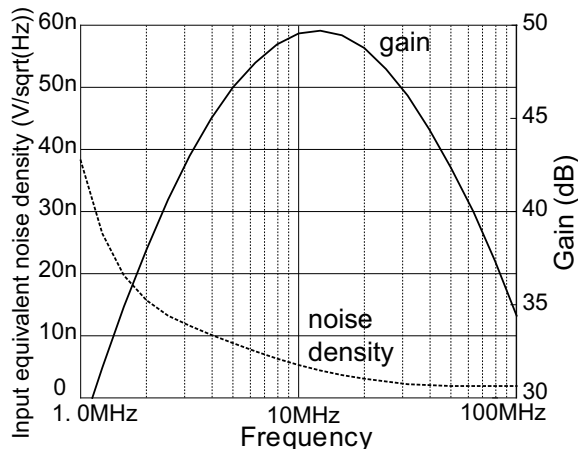


Figure 9: Simulated results for discriminator-block amplifier gain (including LNA gain) and equivalent input noise density, as a function of frequency.

maximum of 1 V by reducing the gain of the variable-gain amplifier and selecting only the lowest gain stage (Large) for the trigger source.

2.2.4. Delay (low-pass filter)

In a self-triggering scheme, charge integration circuits are triggered by the input PMT signal itself. The PMT signal to be integrated must be delayed to locate it in the charge gate, otherwise not whole charge is integrated. In the QTC, we create the necessary delay by using a LPF.

The LPF must have not only a long delay, but also a shorter tail than the charge gate time of 400 ns. A high-order LPF, although ideal for delaying input signals without loss of waveform symmetry, is unduly large because of its many components, especially bulky capacitors. Consequently, the QTC uses a second-order voltage-controlled voltage source (VCVS) LPF whose damping characteristic is comparatively sharp with few components.

Figure 10 shows the circuit diagram of the VCVS LPF. The low-pass cutoff frequency is given by $f_c = 1/(2\pi R_3\sqrt{C_3C_4}) = 6.1$ MHz. The quality factor is given by $Q = \sqrt{(C_4/C_3)}/2 = 0.58$.

Figure 11 compares the simulated waveforms for the VCVS LPF and first-order passive LPF. The VCVS LPF achieves short settling time (~ 200 ns, shorter than the charge gate time) and sufficiently long delay (~ 20 ns, longer than the sum of ~ 15 ns rise-time of PMT signals and ~ 2 ns gate delays in the logic needed to open the integration gate). The output tail of the passive

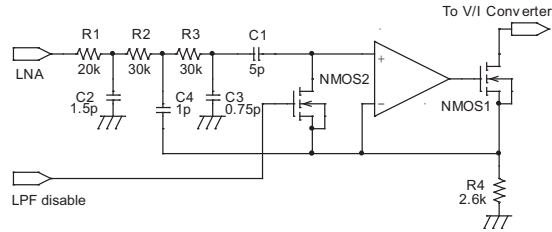


Figure 10: Circuit diagram of the VCVS LPF with positive feedback provided by the capacitor. At the reset period, the "LPF disable" signal closes the NMOS2 switch, and the baseline of the LPF input is restored.

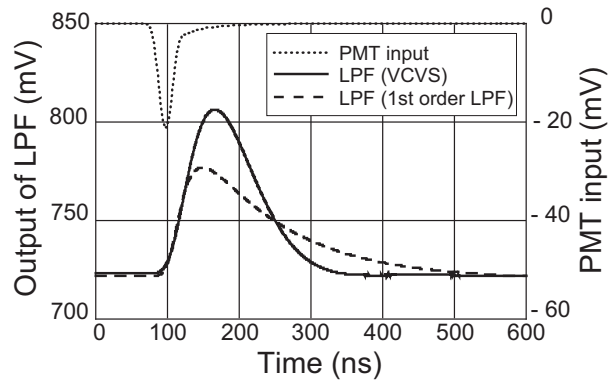


Figure 11: Simulated waveforms for the LPF outputs. The delayed waveforms for the VCVS LPF and the first-order passive LPF are denoted by solid and dashed lines, respectively.

LPF is longer and does not settle within the charge gate time.

The LPF output has equal areas above and below zero volts because of the AC coupling capacitor (C1 in Fig. 10) on the signal line. When the pulse repetition frequency is high compared with the lower cutoff frequency of the capacitor, the system suffers signal droop and baseline wander. To avoid charge-measurement biases for successive PMT signals, we restore the LPF baseline by forcing the signal line to connect to ground during the reset period of every processing cycle.

Since floating capacitors (e.g. C1) are large-area metal-insulator-metal capacitors (MIMCaps), we should be concerned about capacitive couplings with other signal lines. The C1 capacitor has an area of $150 \mu\text{m} \times 45 \mu\text{m}$. If a logic line with a width of $0.8 \mu\text{m}$ is arranged above the capacitor, a parasitic capacitance between them can be as large as 10 fF. Such a large coupling with a logic signal, which rises and falls steeply, could cause serious troubles such as a significant error on a charge measurement or channel crosstalks. The QTC in a developmental stage had a few problems caused by unexpected parasitic couplings. We studied the effect from parasitic couplings using a Focused Ion Beam (FIB), which is one of the microfabrication techniques. The mask design of the QTC ASIC was modified to remove the couplings revealed by the study.

3. Performance

We evaluated the final fabricated QTC chip using a test board on which the QTC ASIC, a TDC [9] and a FPGA are mounted. This section describes the measured charge dynamic ranges, linearities, charge and timing resolutions, channel isolations, ambient temperature dependences, and rate dependences.

Figure 12 shows the performance-evaluation setup. For studies on charge linearity and charge/timing resolution, we used a calibrated programmable charge source (9.2 fC/LSB, 16-bit dynamic range). We prepared three signal paths to achieve a wide range of calibration pulse. To create small signals ($<1 \text{ pC}$, $\sim 1 \text{ mV}$ pulse height) with good signal-to-noise ratio and linearity, we inserted a high-precision wide-band 20-dB attenuator into the signal line. To create large signals above the dynamic range of the charge source, we amplified the signal from the charge source by a custom charge amplifier with dynamic range up to 3000 pC ($\sim 4 \text{ V}$ pulse height) and nonlinearity within $\pm 1\%$. At the merging point, higher-frequency components of the charge

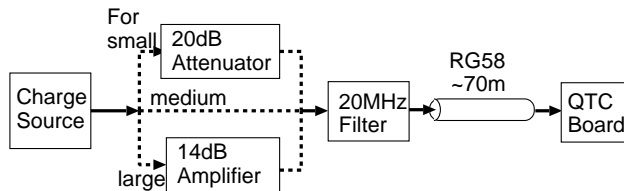


Figure 12: Setup for QTC performance evaluation. Three signal paths are prepared for the three different gain ranges.

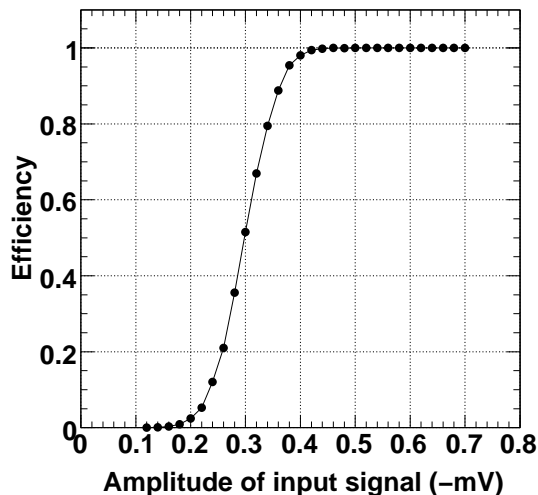


Figure 13: Efficiency curve of the discriminator with -0.3 mV (0.1 p.e.s) threshold.

source signals were filtered by a 70-m RG58 coaxial cable and a 20-MHz low-pass filter to reproduce the actual rise time of the R3600 PMT signal at the SK detector. The charge integration gate was set to 400 ns and the charge dynamic range of the QTC was set to 0.2 – 2500 pC (Table 1). The threshold of the discriminator was set to -0.6 mV unless otherwise noted.

The noise level of the preamplifier and discriminator was tested by counting noise hits in the absence of input signal. No noise hits were observed at -0.3 mV discriminator threshold, equivalent to 0.1 p.e.s and sufficiently below the threshold of 1/4 p.e.s for real experiments.

Figure 13 shows a discriminator efficiency curve at the threshold. The curve’s reasonable shape is due to the good noise performance of the discrim-

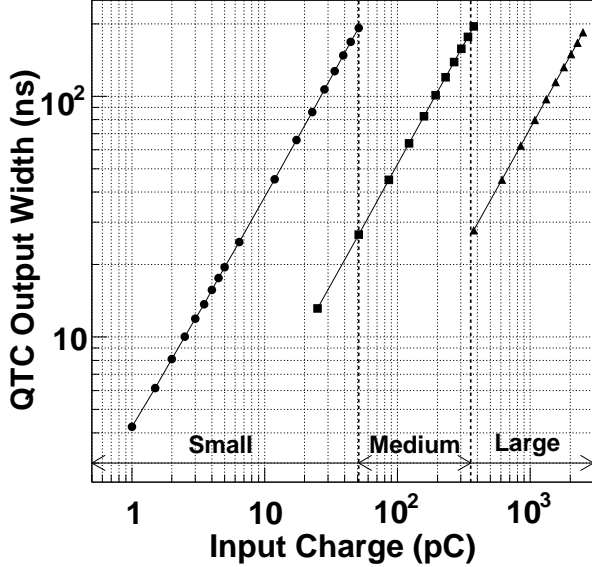


Figure 14: Charge responses of the three QTC ranges as a function of input charge. The vertical axis is the width of the output signal after subtracting the charging time (pedestal). Measurements for the Small, Medium, and Large ranges are denoted by circles, squares, and triangles, respectively. The lowest gain stage (Large) remains unsaturated up to 2500 pC.

inator.

Figure 14 shows outputs of the three QTC ranges as a function of input charge. Each range converts an input charge to an output width with a maximum variance of 200 ns. The lowest gain stage (Large) remains unsaturated up to ~ 3 V, equivalent to 2500 pC.

Figure 15 shows the charge nonlinearity for each gain stage, where non-linearity means deviation from a linear fitted function. The QTC achieves good ($\pm 1\%$) charge linearity over a wide dynamic range, and satisfies our requirements.

Figure 16 shows that the QTC maintains good resolution over a wide dynamic range. The relative charge resolution is $\sim 10\%$ for a single p.e. level (~ 2 pC) and decreases to $< 3\%$ for ≥ 10 pC. The RMS absolute values are about 0.2 pC, almost independent of input charge. These resolutions are sufficiently good compared with the intrinsic charge resolution ($\sim 100\%$) of the R3600 PMTs.

Figure 17 shows the timing resolution of the QTC output signal. The

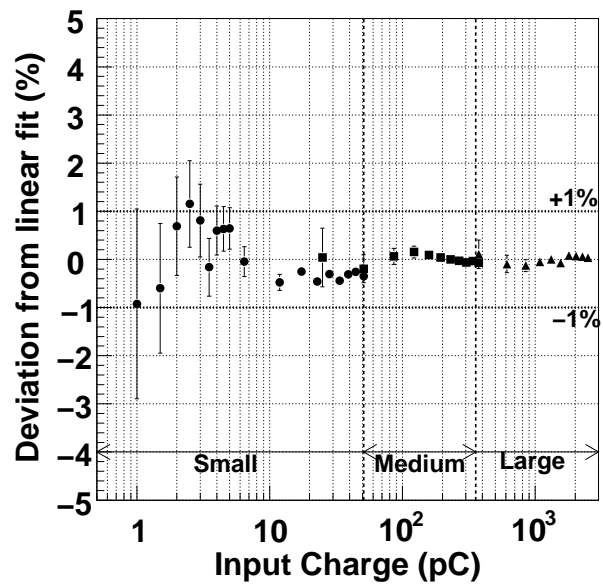


Figure 15: Charge linearity for each QTC gain stage. Measurements for the Small, Medium, and Large ranges are denoted by circles, squares, and triangles, respectively. Nonlinearity is within $\pm 1\%$.

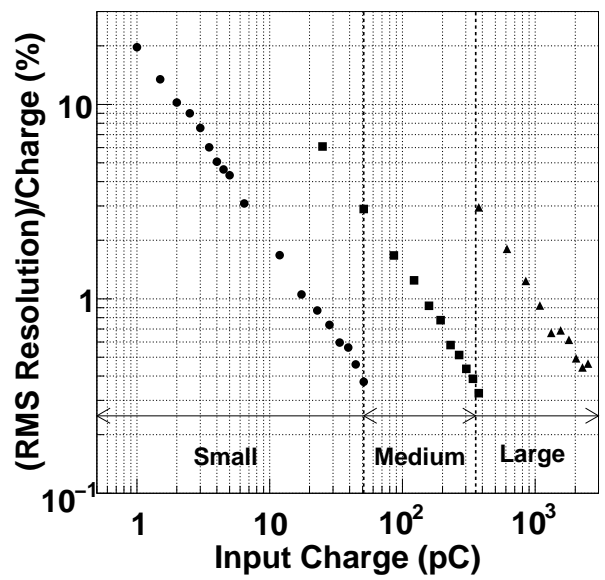


Figure 16: Relative charge resolution (percent). Measurements for the Small, Medium, and Large ranges are denoted by circles, squares, and triangles, respectively. The relative charge resolution varies inversely with input charge because the RMS of the QTC output signal width is almost constant.

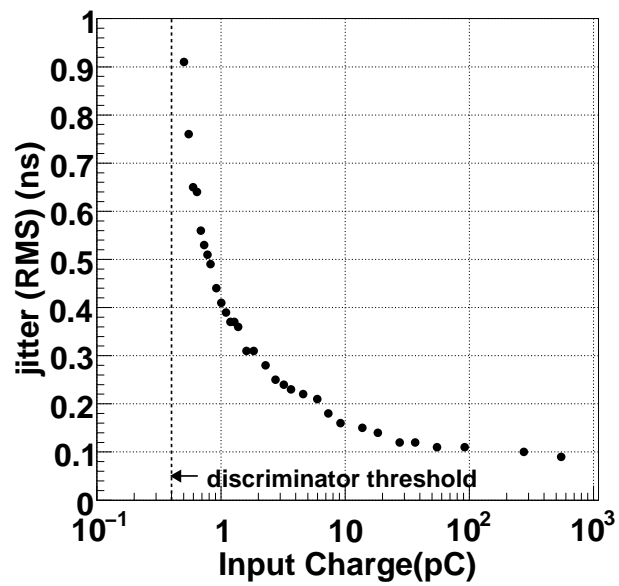


Figure 17: Timing resolution of the QTC output signal. The discriminator threshold (dotted line) is -0.6 mV, equivalent to 0.4 pC. The resolution is well below that of the R3600 PMTs, $2\sim 3$ ns at ~ 2 pC.

timing resolution is the RMS of the leading-edge timing, measured by a 1-GHz digital oscilloscope. The timing resolution for ≥ 100 pC is better than 0.1 ns, consistent with that estimated by the designed noise voltage and slew rate (Section 2.2.3). For smaller signals, resolution increases as the input signal amplitude approaches the discriminator threshold. When the threshold is -0.6 mV, as might be set for real experiments, the timing resolution is 0.3 ns for the single p.e. ($\simeq 2$ pC) level, sufficiently better than the intrinsic timing resolution (2~3 ns) of the R3600 PMTs.

Channel isolation is evaluated by counting hits caused by crosstalk when an input signal is applied to neighboring channels. When the discriminator threshold level for a channel is set to -0.3 mV and -2 V input signal is applied to the neighboring channels, no false hits result from crosstalk. This is sufficient because neighboring channels will also have real hits when a PMT receives a large amount of light.

Figure 18 shows the ambient temperature dependence of QTC charge response, measured in a constant temperature bath. Output width varies linearly with ambient temperature; the coefficients for pedestal data and full-scale charge data are equivalent to -0.15 and -0.30 pC/ $^{\circ}$ C, respectively. The temperature coefficient varies linearly with input charge. This linear relationship enables us to correct for possible ambient temperature changes in real experiments by periodically taking pedestal data ($=0$ pC) as well as calibration data at designated input charges.

Figure 19 shows input rate dependence of the QTC output signal from 10 Hz to 1 MHz. For high-speed signal processing, the input rate dependence must be sufficiently small. For input at the single p.e. (2 pC) level, dependence is <0.5 ns (0.1 pC). Behavior also depends on the width of the QTC output signal in each range. The dependence for 51-pC input, which is full scale for the highest gain stage (Small), is <2 ns, equivalent to 1% change. We thus confirmed that the logic circuits as well as the baseline restoration circuit work as designed.

4. Conclusion

A new high-speed QTC has been developed as a mixed-signal ASIC for PMT readout. Test results show that the QTC satisfies our requirements. The charge and timing resolutions for the single p.e. level are 10% and 0.3 ns, respectively, both better than the intrinsic resolutions of the PMTs. Good charge linearity (1%) is achieved. The discriminator can be operated with a

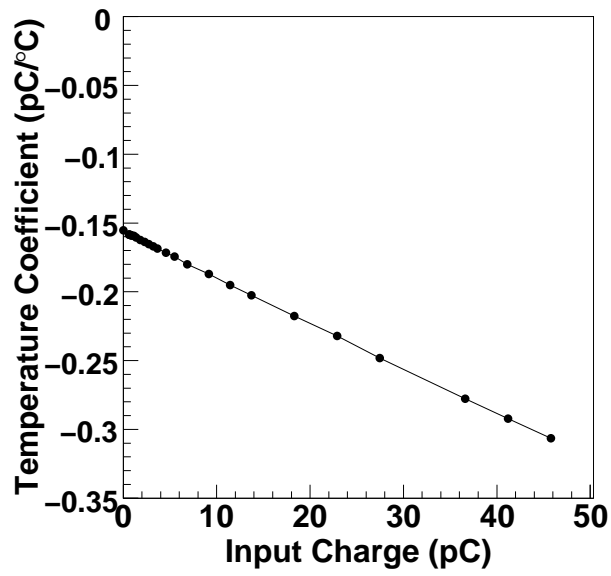


Figure 18: Temperature coefficients for the highest gain stage (Small). Coefficients vary linearly with input charge. Coefficients for the Medium and Large stages are 7 and 49 times, respectively, larger than this.

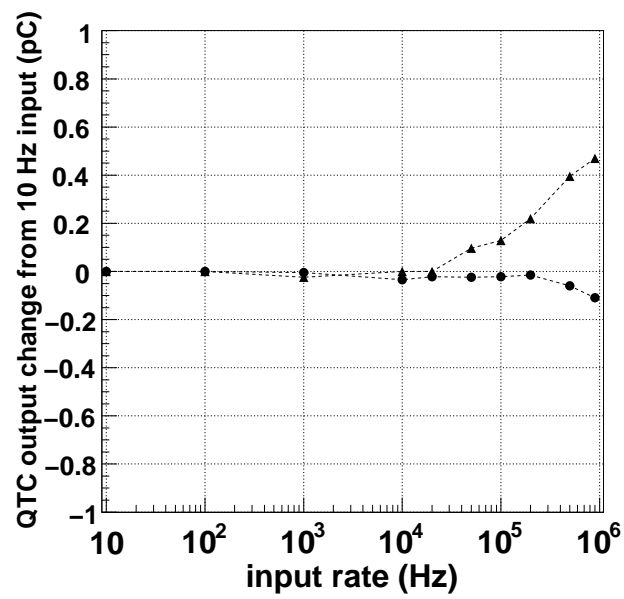


Figure 19: Rate dependence of the QTC output signal as a function of input rate. Changes of output width are <0.5 ns (0.1 pC) and 2 ns (0.5 pC) for input charge of 2 pC (circle) and 51 pC (triangle), respectively.

−0.3 mV threshold, equivalent to 1/10 p.e.s, without suffering from intrinsic electrical noise or channel crosstalk.

In September 2008, we successfully replaced the SK data acquisition electronics with new front-end electronics on which QTCs as reported herein are mounted. Since then, the SK detector has been stable and has operated well. Further results on atmospheric/solar neutrinos, high-intensity accelerator neutrinos, proton decay searches, and more will be reported in the near future.

Acknowledgments

We would like to thank the Super-Kamiokande collaborators for supporting this project and making many helpful discussions. A part of this work was carried out at VLSI Design and Education Center (VDEC), University of Tokyo. This work was partially supported by Research Fellowships of the Japan Society for the Promotion of Science for Young Scientists.

References

- [1] Y. Fukuda *et al.*, Phys. Rev. Lett. 81 (1998) 1562; Y. Ashie *et al.*, Phys. Rev. Lett. 93 (2004) 101801; Y. Ashie *et al.*, Phys. Rev. D 71 (2005) 112005.
- [2] M. B. Smy *et al.*, Phys. Rev. D 69 (2004) 011104; J. Hosaka *et al.*, Phys. Rev. D 73 (2006) 112001.
- [3] Y. Itow *et al.*, hep-ex/0106019 (2001).
- [4] M. Malek *et al.*, Phys. Rev. Lett. 90 (2003) 061101; M. Ikeda *et al.*, Astrophys. J. 669 (2007) 519.
- [5] M. Shiozawa *et al.*, Phys. Rev. Lett. 81 (1998) 3319; Y. Hayato *et al.*, Phys. Rev. Lett. 83 (1999) 1529; K. Kobayashi *et al.*, Phys. Rev. D 72 (2005) 052007; H. Nishino *et al.*, Phys. Rev. Lett. 102 (2009) 141801.
- [6] Y. Fukuda *et al.*, Nucl. Instr. and Meth. A 501 (2003) 418.
- [7] H. Ikeda *et al.*, Nucl. Instr. and Meth. A 320 (1992) 310; T. Tanimori *et al.*, IEEE Trans. Nucl. Sci. NS-36 (1989) 497.

- [8] A. Suzuki *et al.*, Nucl. Instr. and Meth. A 329 (1993) 299.
- [9] Y. Arai *et al.*, Nucl. Instr. And Meth. A 453 (2000) 365.